ResearchGate

See discussions, stats, and author profiles for this publication at: https://www.researchgate.net/publication/220007552

Interfacial Concentration Profiles of Rubbery Polyolefin Lamellae Determined by Quantitative Electron Microscopy

ARTICLE *in* MACROMOLECULES · JANUARY 2008

Impact Factor: 5.8 · DOI: 10.1021/ma071498t

CITATIONS
5

READS
19

7 AUTHORS, INCLUDING:

Enrique Gomez
Pennsylvania State University
77 PUBLICATIONS **1,653** CITATIONS
SEE PROFILE

Christian Kisielowski
Lawrence Berkeley National Laboratory
299 PUBLICATIONS **6,597** CITATIONS
SEE PROFILE

Available from: Christian Kisielowski
Retrieved on: 26 January 2016

Interfacial Concentration Profiles of Rubbery Polyolefin Lamellae Determined by Quantitative Electron Microscopy

Enrique D. Gomez,[†,‡] Megan L. Ruegg,[†] Andrew M. Minor,[§] Christian Kisielowski,[§] Kenneth H. Downing,[||] Robert M. Glaeser,[||,⊥] and Nitash P. Balsara*[,†,‡,#]

Department of Chemical Engineering, University of California, Berkeley, California 94720; Materials Sciences Division, Lawrence Berkeley National Laboratory, Berkeley, California 94720; National Center for Electron Microscopy, Lawrence Berkeley National Laboratory, Berkeley, California 94720; Life Sciences Division, Lawrence Berkeley National Laboratory, Berkeley, California 94720; Department of Molecular and Cell Biology, University of California, Berkeley, California 94720; and Environmental Energy and Technologies Division, Lawrence Berkeley National Laboratory, Berkeley, California 94720

Received July 7, 2007; Revised Manuscript Received October 19, 2007

ABSTRACT: The composition profile across a lamellar phase obtained in a multicomponent blend of saturated poly(butadiene) and poly(isobutylene), stabilized by a saturated poly(butadiene) copolymer serving as a surfactant, was quantified by transmission electron microscopy (TEM) and self-consistent field theory (SCFT). The liquidlike nature of this system at room temperature makes traditional staining methods for the enhancement of contrast ineffective. Instead, we take advantage of the large inelastic scattering cross-section of soft materials to generate contrast in zero-loss TEM images. Independent spatially resolved thickness measurements enable quantification of electron scattering. This enabled a comparison between the TEM data and predictions based on SCFT without any adjustable parameters.

Introduction

Electron microscopy[1−3] and small-angle scattering[4,5] are used extensively for characterizing microstructured polymers. Most studies focus on geometric aspects of the morphological features such as domain size, interdomain distance, and symmetry of the lattice on which the domains reside. There are relatively few studies where the composition of the domains and the composition profiles across the intervening interfaces have been determined.[6−10] For example, analysis of small-angle X-ray scattering (SAXS) data from ordered block copolymer melts is based entirely on the location of the primary and higher order scattering peaks. In principle, the absolute intensity of Bragg scattering peaks can be used to determine the average difference in composition between the domains. This calculation is seldom done because it requires independent knowledge of other factors that affect scattering intensity such as thermal fluctuations, polydispersity, and coherence of the lattice. Quantifying these factors has proven to be an insurmountable challenge for most microstructured polymers. On the other hand, electron microscopy of polymers often requires contrast enhancement by heavy metal staining. The introduction of these metals causes major chemical and physical changes in the material. Chemical changes include cross-linking and chain scission reactions that occur when polymers are exposed to staining agents. Physical changes include contraction of the domains due to cross-linking or expansion of the domains due to the incorporation of staining compounds. Thus, while qualitative comparisons between domain sizes and symmetries obtained by scattering and microscopy are often made, quantitative interpretation of detailed features of the electron micrographs (such as image contrast) is almost always ignored because it is impossible to distinguish between true heterogeneity present in the original sample and that which was introduced during sample preparation. We note in passing that refractive index contrast between micron-sized, unstained phases is routinely obtained by optical microscopy.[11−14]

In spite of the difficulties noted above, there are a few noteworthy experiments where the contrast between phases has been quantified by electron microscopy. Spontak et al. determined the concentration profiles across the interface between microphases of poly(styrene-*block*-butadiene-*block*-styrene) and poly(styrene-*block*-butadiene) copolymers.[9] This enabled quantification of both the width and the sharpness of the density gradients of the interface. The poly(butadiene) microphase in this case was stained with OsO_4, which may deposit nonuniformly and cause imaging artifacts.[15,16] The difficult question of the relationship between the measured profiles and those that existed in the sample prior to staining was left unanswered. Handlin and Thomas took advantage of phase contrast in defocused images of poly(styrene-*block*-isoprene) and poly(styrene-*block*-butadiene) copolymers to generate micrographs of the microstructure without staining. Although quantitative comparisons were not made, qualitative agreement of the experimental contrast with calculated values was found.[17] Siangchaew and Libera used energy-filtered electron microscopy to image the concentration profile across a poly(styrene)/poly(2-vinylpyridine) (PS/PVP) interface in a blend of PS and PVP homopolymers. Because of the presence of the nitrogen atom in PVP and the absence of nitrogen in PS, images were obtained from unstained samples. To our knowledge, this study is the first and only attempt to obtain quantitative information on polymeric domain composition in unstained polymer materials. In the above-mentioned studies, the experimentally obtained profiles were compared with theoretical predictions. A limitation of the methodologies employed in these papers is that com-

[†] Department of Chemical Engineering, UC Berkeley.
[‡] Materials Sciences Division, Lawrence Berkeley National Laboratory.
[§] National Center for Electron Microscopy, Lawrence Berkeley National Laboratory.
[||] Life Sciences Division, Lawrence Berkeley National Laboratory.
[⊥] Department of Molecular and Cell Biology, UC Berkeley.
[#] Environmental Energy and Technologies Division, Lawrence Berkeley National Laboratory.

10.1021/ma071498t CCC: $40.75 © 2008 American Chemical Society
Published on Web 12/08/2007

parisons between theory and experiment required the introduction of one or more adjustable parameters.[9,18]

In this paper, we describe the results of transmission electron microscopy studies on a multicomponent polyolefin blend composed of saturated poly(90% 1,2-butadiene) (homopolymer A), poly(isobutylene) (homopolymer B), and poly(89% 1,2-butadiene-*block*-63% 1,2-butadiene) copolymer (A−C). Our interest in A/B/A−C mixtures stems from the surfactant-like properties of the A−C copolymer which results in the formation of organized, single-phase systems. In the absence of the A−C copolymer, the binary A/B mixture separates into two coexisting macrophases. Small-angle neutron scattering (SANS) data obtained from an A/B/A−C blend with homopolymer A volume fraction of 0.29 and B volume fraction of 0.41 indicate the presence of a lamellar phase. Our objective in this paper is to determine the composition profiles within the lamellar phase and thereby determine the concentration profile and width of the interface by transmission electron microscopy (TEM). The micrographs are obtained without staining. Because of the fact that the empirical formula of all of the components is CH_2 (ignoring deuterium substitution for the moment as it is irrelevant for electron microscopy), we can only obtain the spatial distribution of these elements and not that of the individual polymer components. Contrast in electron micrographs can arise due to diffraction, atomic mass differences, and phase interference. In amorphous materials such as the polymer blend of interest, diffraction effects are not important, and atomic mass differences dominate at zero defocus. We combine the well-established concept of Rutherford scattering,[19] known electron scattering properties of hydrocarbon materials,[3,20] and self-consistent field theory (SCFT) of inhomogeneous polymers[21] to compute the expected contrast from our blend in an electron micrograph. Comparisons between predictions and experiments are presented without resorting to any adjustable parameters.

Materials and Methods

In the A/B/A−C polymer blends, component A was saturated poly(butadiene) with 89% 1,2-addition (sPB89), component B was poly(isobutylene) (PIB), and component C was saturated poly(butadiene) with 63% 1,2-addition (sPB63). The surfactant is an A−C copolymer which we label sPBPB. The prefix "s" in sPB63, sPB89, or sPBPB stands for "saturated" and is replaced by "h" or "d" when we wish to specify whether the polymer is hydrogenated or deuterated. Poly(isobutylene) and poly(butadiene) with varying % 1,2-addition are synthesized using methods described previously, and the poly(butadiene)s are saturated with either deuterium or hydrogen.[22,23] The polymers are characterized using known methods to determine the density, weight-averaged molecular weight, polydispersity index, and % 1,2-addition (for the saturated poly(butadiene) polymers).[22] The structures of the polymers used are shown in Figure 1, and their characteristics are listed in Table 1.

The composition of the blend used in this study in terms of volume fractions is 0.29 dPB89, 0.41 PIB, and 0.30 hPBPB (surfactant). We call this blend B30, the same nomenclature as that used in ref 23. Blends for SANS and TEM were created using methods described in ref 22. Samples were annealed at 90 °C under vacuum for 48 h and then stored at room temperature for several days. We are only concerned with the equilibrium morphology of B30 at room temperature. The coherent SANS intensity, I, vs scattering vector, q ($q = 4\pi \sin(\theta/2)/\lambda$, θ is the scattering angle and λ is the neutron wavelength), of B30 used in this paper is similar to data presented in ref 23, where details concerning data acquisition and analysis may be found.

TEM samples were made by quenching the blend into liquid nitrogen and transferring the frozen sample into an RMC Boeckeler PT XL Ultramicrotome operating at 173 K using a cryogenic attachment. Sections were collected on a carbon/Formvar-coated grid. The presence of the grid coating (thickness typically 0.05 × mean free path) was ignored for all of our analysis. Grids were immediately taken into a Gatan cryostage of a Zeiss LIBRA 200FE transmission electron microscope. Although the samples were transferred at room temperature, the stage was cooled to 173 K within 30 min. All micrographs were taken at 101 K.

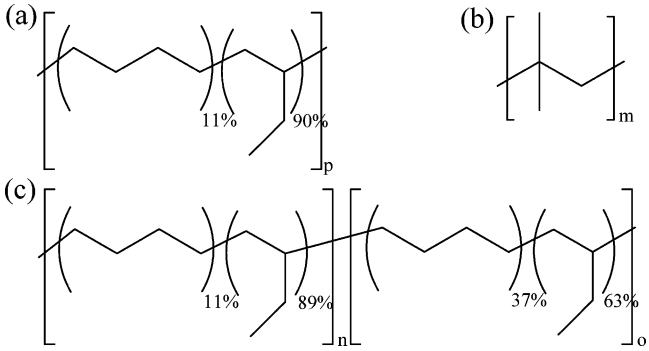

Figure 1. Chemical structure of the components of the polymer blend used in this study: (a) saturated poly(90% 1,2-butadiene), (b) poly(isobutylene), and (c) diblock copolymer surfactant.

The LIBRA 200FE microscope used in this study is equipped with a field-emission gun, Kohler illumination system, and a post-specimen, in-column Omega energy filter. It was operated at 200 kV, and the incident energy dispersion was ~1 eV. Two types of images were collected: bright field and thickness maps. Bright field images were taken with zero defocus (or nearly so). Thickness maps were generated by taking the log of the ratio of the unfiltered image to the zero-loss energy-filtered image, resulting in position-dependent relative thicknesses (thickness divided by the mean free path). All images were captured on a 2k × 2k CCD camera, normalized for detector gain variations, and corrected for dark counts. The micrographs used in this study were taken at doses $<10^5$ e^-/nm^2. We show that radiation damage is not important for the length scales studied in this work.

The primary driving force for working with unstained samples was that all of our attempts to preferentially stain the sample failed. The processes by which staining materials are absorbed in different polymeric species are qualitatively understood. In some cases stains are absorbed due to the presence of specific chemical moieties, for example, when OsO_4 is used to stain polymers containing C=C double bonds. In other cases, differences in stain concentration occur due to differences in the diffusion coefficient of the staining agent, as in when RuO_4 is used to stain the amorphous phase in blends of amorphous and crystalline polymers.[2] Since PIB is known to be a barrier for the diffusion of small molecules such as oxygen, we thought that this may lead to contrast in our sample. In addition, the quaternary carbon atom in PIB is more susceptible to chemical attack than the other carbon atoms, and this could also, in principle, lead to differentiation between the lamellae. Another difficulty with our A/B/A−C blend is that all of the components are rubbery at room temperature. Thus, exposure of the thin sections to staining compounds results in rearrangement and collapse of the sample, preventing TEM imaging. In spite of trying a broad range of staining protocols (including staining prior to sectioning), we were unable to obtain nonuniform stain distributions in our samples.

Self-Consistent-Field Theory

Our methods for utilizing self-consistent field theory (SCFT) to describe the thermodynamic properties of multicomponent A/B/A−C blends have been previously discussed.[22] The only input parameters needed are Flory−Huggins interaction parameters for three binary blends ($\chi_{A,B}$, $\chi_{A,C}$, and $\chi_{B,C}$) and the statistical segment lengths for each of the components (l_A, l_B, and l_C). These values have been previously determined and tabulated from homogeneous binary blends.[23] Our SCFT

Table 1. Characteristics of Polymers

label	polymer	MW (kg/mol)	PDI[a]	density (g/cm^3)	T_g (K)
dPB89	deuterated 90% 1,2-poly(butadiene)	36.5	1.02	0.904	240[d]
PIB	poly(isobutylene)	18.7	1.02	0.913	201[e]
block 1 of hPBPB	hydrogenated 89% 1,2-poly(butadiene)	126		0.863[c]	239[d]
block 2 of hPBPB	hydrogenated 63% 1,2-poly(butadiene)	178	1.02[b]	0.862[c]	219[d]

[a] Polydispersity index. [b] PDI is for the entire block copolymer. [c] Densities are interpolated from a series of polymers with varying % 1,2-addition. [d] From ref 45. [e] From ref 46.

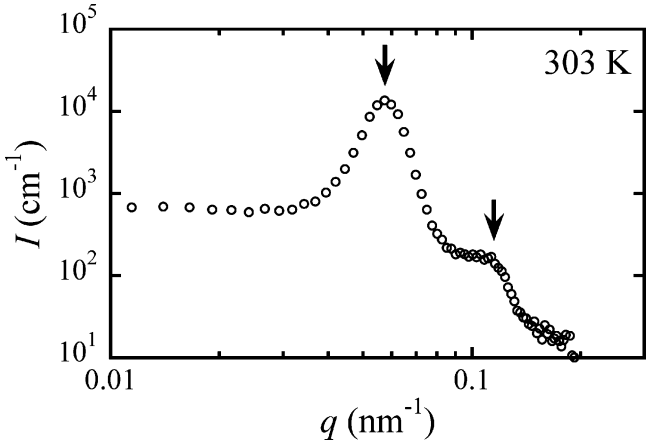

Figure 2. SANS intensity vs scattering vector, q, of blend B30. The arrows denote q^* and $2q^*$.

calculations are carried out in one dimension, and we neglect the effects of concentration fluctuations.

Analysis of Image Contrast in Amorphous Polymer Blends

In the absence of diffraction or phase contrast, bright field images are created by the forward-scattered beam, and contrast is generated by removing scattered electrons at angles defined by an objective aperture at the back focal plane. Although the intensities of both inelastically and elastically scattered electrons have an angular dependence, inelastically scattered electrons scatter preferentially at lower angles and thus are removed less effectively with the objective aperture.[24] After the first demonstration of energy-filtered imaging by Castaing and Henry,[25] it became possible to create images without inelastically scattered electrons. Zero-loss energy filtering, where inelastically scattered electrons are selectively removed, is used to improve image quality, since inelastically scattered electrons are subject to the chromatic aberration of the microscope.[26] The inelastic scattering cross-section is larger than the elastic cross-section for soft hydrocarbon samples probed with incident electron beams with energies between 100 and 300 keV. The contrast in TEM bright field images can thus be significantly enhanced by removing inelastically scattered electrons.[24] Kunz et al. have shown qualitatively that zero-loss imaging can increase the contrast for copolymers.[27]

Our analysis begins with an objective aperture and energy filter that transmit electrons with energy $E = \{E_0 - \Delta E/2, E_0 + \Delta E/2\}$ and a scattered angle less than β. E_0 is the incident energy, 200 keV in our case. We assume a monoenergetic parallel illumination and zero defocus. The ratio of the intensity of the transmitted beam, I, to that of the incident beam, I_0, is given by

$$\frac{I}{I_0} = \exp(-Qt) \tag{1}$$

where Q has units of 1/length and t is the thickness of the specimen. Q is the inverse of the mean free path. Equation 1 is analogous to Beer's law for optical absorption, making Q akin to an absorption coefficient. In the electron microscopy literature, Q is often called the total scattering cross-section.[19,28] In principle, both Q and t vary across the specimen. For interactions between electrons and a compound with molecular weight M and density ρ, Q is given by[19,28]

$$Q = \frac{N_0 \sigma_{\mathrm{mol}}(\beta,E)\rho}{M} \tag{2}$$

where N_0 is Avogadro's number and $\sigma_{\mathrm{mol}}(\beta,E)$ is the molecular scattering cross-section (units length^2), which depends on the collection angle β and allowed energies, E. Note that M and σ_{mol} must be defined consistently, and in the case of polymers it is convenient to define them on the basis of the chemical repeat units. In our case, these units are defined in Figure 1. σ_{mol} is composed of the sum of both elastic and inelastic components. The elastic cross-section, σ_e, can be calculated using a modified Rutherford equation,[19] and the inelastic scattering cross-section, σ_i, can be calculated using[24]

$$\frac{\sigma_i}{\sigma_e} = \frac{k}{Z_j} \tag{3}$$

k is approximately a constant. In refs 29 and 30, a combined theoretical and experimental approach estimated k to be about 14 for the nucleic acid base adenine, and separate experiments using poly(styrene) support $k = 14$.[31] k, however, varies in the literature from 10 to 25,[20,24,30,32−39] making reliable calculation of σ_{mol} difficult.

For a multicomponent system, Q is given by a straightforward extension of eq 2.

$$Q(x,y) = N_0 \sum_i \frac{\rho_i}{M_i} \sigma_{\mathrm{mol},i}(\beta,E;x,y)\, \phi_i(x,y) \tag{4}$$

x and y are axes of a Cartesian reference frame located in the plane of the sample, and z corresponds to the direction along the incident electron beam. In eq 4, we explicitly show parameters that depend on position in the specimen (x,y). Images are projections along z, and all parameters must be averaged over the thickness of the specimen. $\phi_i(x,y)$ is the volume fraction of the ith component as a function of position. The molecular scattering cross-sections of polymeric materials are often very similar. For the particular sample studied here, they are identical since the empirical formula of all components is CH_2. So if we assume a constant thickness, t, and a constant σ_{mol}

$$\frac{I(x,y)}{I_0} = \exp\left(-tQ_{\mathrm{AVG}}\upsilon_{\mathrm{AVG}} \sum_i \frac{\rho_i}{M_i} \phi_i(x,y)\right) \tag{5}$$

Note that by measuring $(Qt)_{\mathrm{AVG}}$ the intensity and contrast can be calculated without needing to compute σ_{mol}. υ_{AVG} is the average molar volume given as

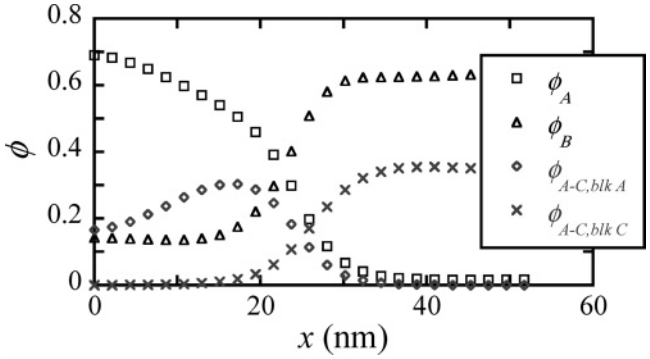

Figure 3. Volume fraction profiles of the different components in blend B30 as a function of *x*, the distance along the lamellae normal. Polymer A is deuterated poly(90% 1,2-butadiene); polymer B is poly(isobutylene); A−C, blk A is the poly(89% 1,2-butadiene) block of the copolymer surfactant; and A−C, blk C is the poly(63% 1,2-butadiene) block of the copolymer.

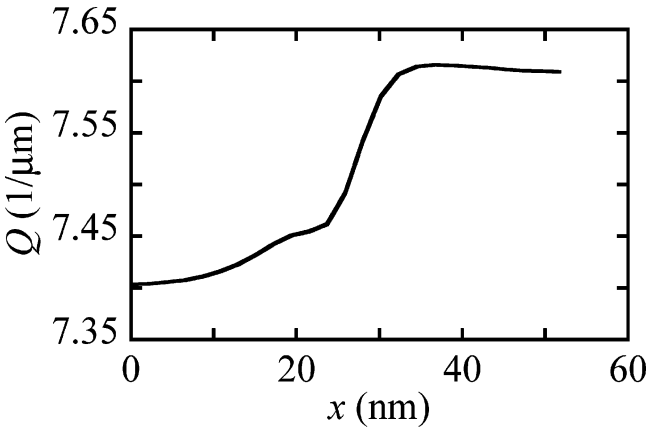

Figure 4. *Q* across the lamellar interface for B30 calculated using SCFT volume fractions from Figure 3, eq 4, parameters from Table 1, and $\sigma_{mol} = 8.12 \times 10^{-4}$.

$$v_{AVG} = \sum_i \frac{M_i}{\rho_i} \bar{\phi}_i \tag{6}$$

where $\bar{\phi}_i$ is the average volume fraction of component *i* in the sample. Averages are taken over all space (*x*, *y*, *z*).

The contrast, *C*, between two homogeneous phases labeled 1 and 2, in the limit of low contrast, is given by

$$C = \frac{\Delta I}{\bar{I}} = N_0 \sigma_{mol}(\beta,E) t \left(\frac{\rho_1}{M_1} - \frac{\rho_2}{M_2}\right) = (Qt)_{AVG} v_{AVG} \left(\frac{\rho_1}{M_1} - \frac{\rho_2}{M_2}\right) \tag{7}$$

Results and Discussion

Figure 2 shows the SANS intensities, $I(q)$, vs scattering vector, q, for blend B30 at 303 K (approximately room temperature). The primary peak (q^*) occurs at 0.0573 nm^{-1}, and the secondary peak lines up closely with $2q^*$, as seen by the arrows in Figure 2. The SANS data of B30 indicate the presence of a lamellar morphology with a periodicity of 110 nm. Because of lack of knowledge regarding effects such as average grain size, Debye−Waller factors, etc., it is not possible to obtain quantitative estimates of the composition profile across the lamellae from the SANS data. An attempt to obtain such information is presented in a related study,[22] where the relative intensities of the primary and second-order SANS peaks as a function of temperature of a similar blend are compared to predictions made from the Fourier transforms of volume fraction profiles obtained using SCFT.

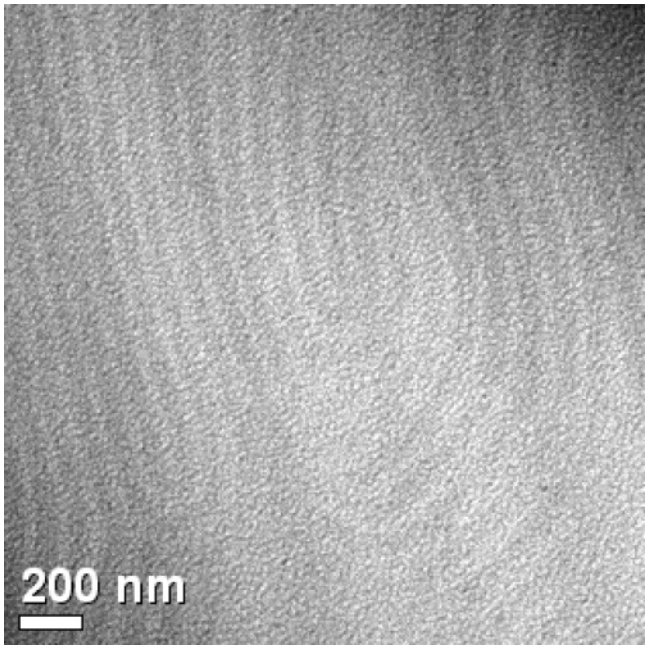

Figure 5. TEM micrograph of the polymer blend B30. An 8 eV spectrometer slit was used. No staining was performed on the sample.

In Figure 3, we show the volume fraction profiles of the components across the interface of the lamellae determined by SCFT calculations. The SCFT calculations predict a domain spacing of 103 nm, in reasonable agreement with our scattering data (110 nm, Figure 2). Using these volume fraction profiles, we calculate $Q(x)$ using eq 4, with densities from Table 1 and σ_{mol} calculated by methods described in ref 24 ($\sigma_{mol} = 8.12 \times 10^{-4}$ nm^2). *x* is the Cartesian coordinate directed along the normal to the lamellae. The resulting $Q(x)$ from the middle of one lamella to the middle of the adjacent lamella is shown in Figure 4. Note that the calculated size of the lamellae is in quantitative agreement with experiments, and the maximum variation of $Q(x)$ is about 3%.

Figure 5 is a bright field TEM image of B30 taken close to zero defocus with an energy filter slit width of 8 eV, no objective aperture, and without any staining. A periodic lamellar phase with a +1/2 dislocation is visible in the micrograph. The period of the lamellar phase is about 100 nm, which is consistent with SANS and SCFT results given above. From eq 7, it is evident that the contrast between lamellae comes from the difference in molar volume between the two phases. In the micrograph of Figure 5, the dark phase is PIB, since the PIB-rich phase has a larger density (Figure 3 and Table 1). To our knowledge, this is the first electron micrograph of a polymer blend composed entirely of components that are rubbery at room temperature. Phase contrast microscopy, where differences in the phase of the scattered beam generate contrast, is ineffective for enhancing the contrast of structures with large periodicities.[17,40,41] For materials with a characteristic spacing of 100 nm, such as the polymer blend studied here, the amount of defocus necessary to significantly improve the contrast is large. A defocus of 100 μm, already unacceptable for imaging, would only improve contrast by about 8% (the contrast would increase from, for example, 1% to 1.08%).[28]

In order to quantify our results using eq 5, we need to obtain *t* and *Q* of our sample. The spatially resolved product *Q* and *t*, or "thickness map", can be calculated by taking the ratio of two images, an unfiltered image and a zero-loss filtered image,[24] since

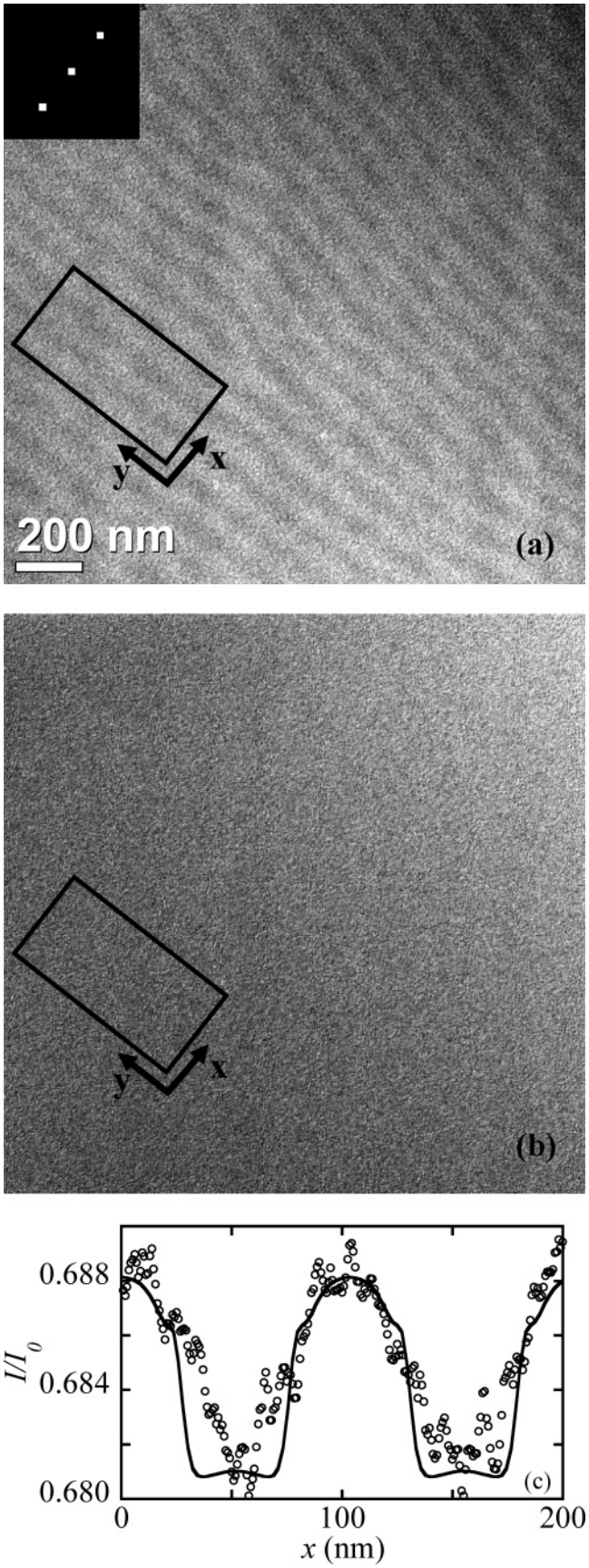

Figure 6. (a) TEM micrograph of B30. The inset is the local FFT of the image within the black box. (b) Thickness map of the same region as (a). (c) Experimental (open circles) and theoretical (solid line) normalized interfacial profiles calculated using eq 4 and (a) and (b). The abscissa (x) is in nm perpendicular to the lamellae. Black boxes in (a) and (b) denote areas used to generate profiles for (c).

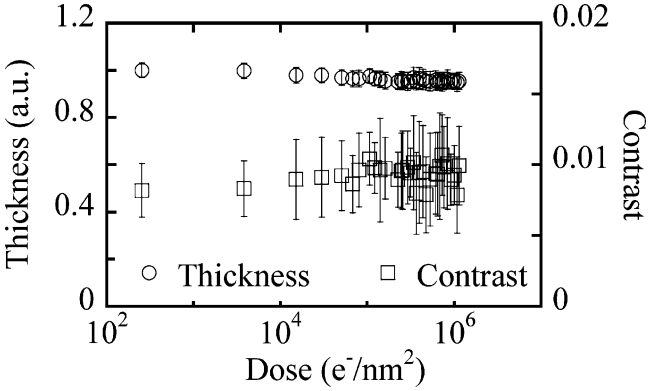

Figure 7. (a) Contrast and sample thickness as a function of dose. There is no perceptible change in the contrast and a small decrease in the thickness. The error bars are the standard deviation of the measurement for a single image.

$$Qt = \ln\left(\frac{I_T}{I_{ZL}}\right) \tag{8}$$

I_T is the total intensity integrated over all energies, and I_{ZL} is the intensity of the zero-loss electrons. An 8 eV post-specimen energy slit was used, but no objective aperture. We assume that unfiltered images capture all of the inelastically scattered electrons and that zero-loss images contain no inelastically scattered electrons. Figure 6a is a bright field micrograph of the lamellar structure, and Figure 6b is the corresponding thickness map. Figures 6a and 6b were taken at a dose of about 10^4 e^-/nm^2. The average value of Qt obtained by integrating over Figure 6b, $(Qt)_{AVG}$, is 0.401 ± 0.038. In most of the micrographs, our thickness maps are featureless as shown in Figure 6b, even though there is a periodic variation in Q. This is probably due to the high noise level in thickness maps (about 10%),[42] which is significantly higher than the expected variation in Q (3%). Our bright field images typically have a noise level of less than 1%.

The thickness of the sample can be determined from $(Qt)_{AVG}$ by calculating Q_{AVG}. Q_{AVG} can be obtained from eq 2 using the parameters in Table 1 and the molecular scattering cross-section, σ_{mol}, which can be calculated by following ref 24. We obtain $\sigma_{mol} = 8.12 \times 10^{-4}$ nm^2, resulting in $Q_{AVG} = 0.007\,98$ nm^{-1} (mean free path = 125 nm), which yields $t_{AVG} = 50$ nm. σ_{mol}, however, can vary from 5.92×10^{-4} to 1.48×10^{-3} nm^2 due to the uncertainty in measuring the ratio between the elastic and inelastic cross-section (see eq 3 and subsequent discussion following eq 3). Although we have no independent measurement of the actual thickness of the sample, we note that the microtome sectioning thickness was set to 50 nm. The quantitative agreement between these two values is probably fortuitous.

In Figure 6a, we show one micrograph selected for comparison between theory and experiment.[43] The boxes in Figures 6a and 6b denote the experimental data used. The orientation of the box was determined by the local Fourier transform of the data within the box, shown in the inset of Figure 6a. Integration of the thickness map (Figure 6b) of this region yields $(Qt)_{AVG} = 0.379 \pm 0.029$ ($t_{AVG} = 47$ nm). Using our SCFT results (Figure 3), parameters from Table 1, and $(Qt)_{AVG} = 0.379$ enables the calculation of the normalized intensity, $I(x)/I_0$, using eq 5 (the x direction is defined in Figures 6a and 6b). The solid curve in Figure 6c is the result of this calculation. The open circles in Figure 6c are experimentally determined $I(x)/I_0$ values after integration over 425 pixels along the y direction in the box of Figure 6a. The incident intensity, I_0, was determined by spatially averaging over the intensity of a bright field image

obtained from an empty region of the grid. The agreement between theory and experiment is reasonable and provides support for the theoretically predicted composition profiles of the components presented in Figure 3. Qualitatively similar results are obtained for other images of B30, and these results are presented in the Supporting Information.

The contrast in our images, C_{exp}, was determined from Figure 6a by first fitting Gaussians around the local maxima and minima of the experimental intensity profile (Figure 6c). $C_{exp} = 1.1 \pm 0.1\%$ was calculated by taking the difference of the maxima and minima, which is then divided by the average intensity, as defined in eq 7. Our theoretical contrast, $C = 1.1\%$, was calculated using eq 7 with $(Qt)_{AVG} = 0.379$ determined from our thickness map (boxed area in Figure 6b) and parameters from Table 1. The difference in molar volume between the two phases was calculated using our SCFT results (Figures 3 and 4).

To explore the effect of radiation damage on contrast, we monitored the mass thickness and contrast as a function of dose, and these results are shown in Figure 7. Thickness and contrast values were obtained by averaging thickness maps and bright field images, respectively, over the same region (about 30 lamellae). Contrast was calculated in the same manner as in the preceding paragraph. In Figure 7, there is a 5% decrease in the thickness of the sample when the dose is increased from 10^2 to 10^6 e^-/nm^2, while the contrast is constant within experimental error over that range of dose. This is consistent with previous reports that at around 100 K the mass loss of poly(isobutylene) and saturated poly(butadiene) occurs at a similar rate while exposed to high-energy radiation.[44] Thus, the small amount of mass loss could be either sublimation of frozen water due to contamination or isotropic mass loss due to chain damage. In either case, we conclude that radiation damage does not have a significant effect on our results.

Conclusions

The lamellar microstructure of an unstained polyolefin blend composed of components that are rubbery at room temperature was imaged using zero-loss energy filtered electron microscopy. This enables determination of the composition profile across the lamellar interfaces. The experimentally determined composition profiles are in agreement with predictions based on self-consistent field theory. This agreement is obtained without resorting to any adjustable parameters.

Acknowledgment. This work was conducted within the Electron Microscopy of Soft Matter Program at Lawrence Berkeley National Laboratory and supported by the Director, Office of Science, Office of Basic Energy Sciences, Materials Sciences and Engineering Division, of the U.S. Department of Energy under Contract DE-AC02-05CH11231. TEM work was done at The National Center for Electron Microscopy, Lawrence Berkeley National Laboratory, U.S. Department of Energy, and is supported under Contract DE-AC02-05CH11231. The facilities at NIST are supported in part by the National Science Foundation under Agreement DMR-9986442. The authors thank Sam Gido for initial training on microtoming and electron microscopy of polymers.

Supporting Information Available: Supplemental bright field TEM images, thickness maps, and comparisons between experimental and theoretical TEM intensity profiles. This information is available free of charge via the Internet at http://pubs.acs.org.

References and Notes

(1) Fultz, B.; Howe, J. M. *Transmission Electron Microscopy and Diffractometry of Materials*, 2nd ed.; Springer: Berlin, 2002.
(2) Sawyer, L. C.; Grubb, D. T. *Polymer Microscopy*, 2nd ed.; Chapman & Hall: London, 1996.
(3) Thomas, E. L. In *The Structure of Crystalline Polymers*; Hall, I. H., Ed.; Applied Science: Essex, UK, 1984; pp 79−124.
(4) Roe, R.-J. *Methods of X-ray and Neutron Scattering in Polymer Science*; Oxford University Press: New York, 2000.
(5) Higgins, J. S.; Benoit, H. C. *Polymers and Neutron Scattering*; Oxford University Press: New York, 1994.
(6) Galloway, J. A.; Montminy, M. D.; Macosko, C. W. *Polymer* **2002**, *43*, 4715−4722.
(7) Torikai, N.; Noda, I.; Karim, A.; Satija, S. K.; Han, C. C.; Matsushita, Y.; Kawakatsu, T. *Macromolecules* **1997**, *30*, 2907−2914.
(8) Karim, A.; Slawecki, T. M.; Kumar, S. K.; Douglas, J. F.; Satija, S. K.; Han, C. C.; Russell, T. P.; Liu, Y.; Overney, R.; Sokolov, O.; Rafailovich, M. H. *Macromolecules* **1998**, *31*, 857−862.
(9) Spontak, R. J.; Williams, M. C.; Agard, D. A. *Macromolecules* **1988**, *21*, 1377−1387.
(10) Harper, P. E.; Mannock, D. A.; Lewis, R.; McElhaney, R. N.; Gruner, S. M. *Biophys. J.* **2001**, *81*, 2693−2706.
(11) Chastek, T. Q.; Lodge, T. P. *J. Polym. Sci., Part B: Polym. Phys.* **2006**, *44*, 481−491.
(12) Chastek, T. Q.; Lodge, T. P. *Macromolecules* **2003**, *36*, 7672−7680.
(13) Balsamo, V.; vonGyldenfeldt, F.; Stadler, R. *Macromol. Chem. Phys.* **1996**, *197*, 3317−3341.
(14) Albuerne, J.; Marquez, L.; Muller, A. J.; Raquez, J. M.; Degee, P.; Dubois, P.; Castelletto, V.; Hamley, I. W. *Macromolecules* **2003**, *36*, 1633−1644.
(15) Wolosewick, J. J.; Porter, K. R. *J. Cell Biol.* **1979**, *82*, 114−139.
(16) Smith, R. W. *Microsc. Microanal., Suppl. S02* **2002**, *8*, 190−191.
(17) Handlin, D. L.; Thomas, E. L. *Macromolecules* **1983**, *16*, 1514−1525.
(18) Siangchaew, K.; Libera, M. *Macromolecules* **1999**, *32*, 3051−3056.
(19) Williams, D. B.; Carter, C. B. *Transmission Electron Miscroscopy*; Plenum Press: New York, 1996.
(20) Reimer, L. *Transmission Electron Microscopy*; Springer-Verlag: Berlin, 1993.
(21) Fredrickson, G. H. *The Equilibrium Theory of Inhomogeneous Polymers*; Oxford University Press: New York, 2006.
(22) Reynolds, B. J.; Ruegg, M. L.; Balsara, N. P.; Radke, C. J.; Shaffer, T. D.; Lin, M. Y.; Shull, K. R.; Lohse, D. J. *Macromolecules* **2004**, *37*, 7401−7417.
(23) Ruegg, M. L.; Reynolds, B. J.; Lin, M. Y.; Lohse, D. J.; Balsara, N. P. *Macromolecules* **2006**, *39*, 1125−1134.
(24) Egerton, R. F. *Electron Energy-Loss Spectroscopy in the Electron Microscope*, 2nd ed.; Plenum Press: New York, 1996.
(25) Castaing, R.; Henry, L. *C. R. Hebd. Acad. Sci.* **1962**, *255*, 76.
(26) Grimm, R.; Typke, D.; Baumeister, W. *J. Microsc. (Oxford, U.K.)* **1998**, *190*, 339−349.
(27) Kunz, M.; Moller, M.; Cantow, H. J. *Makromol. Chem., Rapid Commun.* **1987**, *8*, 401−410.
(28) Heidenreich, R. D. *Fundamentals of Transmission Electron Microscopy*; John Wiley & Sons: New York, 1964.
(29) Langmore, J. P.; Wall, J.; Isaacson, M. S. *Optik* **1973**, *38*, 335−350.
(30) Wall, J.; Isaacson, M.; Langmore, J. P. *Optik* **1974**, *39*, 359−374.
(31) Du Chesne, A. *Macromol. Chem. Phys.* **1999**, *200*, 1813−1830.
(32) Lenz, F. *Z. Naturforsch. A* **1954**, *9*, 185−204.
(33) Inokuti, M.; Dehmer, J. L.; Baer, T.; Hanson, J. D. *Phys. Rev. A* **1981**, *23*, 95−109.
(34) Egerton, R. F. *Phys. Status Solidi A* **1976**, *37*, 663−668.
(35) Reimer, L.; Rossmessemer, M. *J. Microsc. (Oxford, U.K.)* **1990**, *159*, 143−160.
(36) Brunger, W.; Menz, W. *Z. Phys.* **1965**, *184*, 271.
(37) Lippert, W. *Naturwissenschaften* **1963**, *50*, 219.
(38) Badde, H. G.; Kappert, H.; Reimer, L. *Z. Angew. Phys.* **1970**, *30*, 83.
(39) Burge, R. E.; Misell, D. L.; Smart, J. W. *J. Phys. C: Solid State Phys.* **1970**, *3*, 1661.
(40) Roche, E. J.; Thomas, E. L. *Polymer* **1981**, *22*, 333−341.
(41) Handlin, D. L.; Thomas, E. L. *J. Mater. Sci. Lett.* **1984**, *3*, 137−140.
(42) The noise in the thickness maps was significantly higher than in our bright field images because of the large amount of noise in the unfiltered images used to generate the thickness maps.
(43) We take the FFT of all of our images and find the minimum periodicity, d_{min}, which we take to be the *d*-spacing of our sample (101 nm). Prior to quantitative analysis, we reject all images which show a *d*-spacing larger than 10% of d_{min}, since these are lamellae which are not

perpendicular to the electron beam. The *d*-spacing of Figure 6a, obtained from the FFT in the inset, is 104 nm.
(44) Chapiro, A. *Radiation Chemistry of Polymeric Systems*; John Wiley & Sons: New York, 1962.
(45) Krishnamoorti, R. Ph.D. Dissertation, Princeton University, 1994.
(46) Brandrup, J., Immergut, E. H., Grulke, E. A., Abe, A., Bloch, D. R., Eds. *Polymer Handbook*, 4th ed.; John Wiley & Sons: New York, 2005.

MA071498T